Tailoring Porosity and Rotational Dynamics in a Series of Octacarboxylate Metal-Organic Frameworks

Florian Moreau,[a] Daniil I. Kolokolov,[b,c] Alexander G. Stepanov,[b,c] Timothy L. Easun,[d] Anne Dailly,[e] William Lewis,[f] Alexander J. Blake,[f] Harriott Nowell,[g] Matthew J. Lennox,[f] Elena Besley,[f] Sihai Yang[a]* and Martin Schröder [a,h]*

[a]   School of Chemistry, University of Manchester, Oxford Road, Manchester M13 9PL, U.K.

[b]   Boreskov Institute of Catalysis, Siberian Branch of Russian Academy of Sciences, Prospekt Akademika Lavrentieva 5, Novosibirsk 630090, Russia.

[c]   Novosibirsk State University, Pirogova Street 2, Novosibirsk 630090, Russia.

[d]   School of Chemistry, Cardiff University, Main Building, Park Place, Cardiff CF10 3AT, U.K.

[e]   General Motors Global Research and Development Center, Warren, MI, USA

[f]   School of Chemistry, University of Nottingham, University Park, Nottingham NG7 2RD, U.K.

[g]   Diamond Light Source, Harwell Science Campus, Oxon, OX11 0DE, UK.

[h]   Nikolaev Institute of Inorganic Chemistry, Siberian Branch of the Russian Academy of Sciences, 3 Acad. Lavrentiev Ave., Novosibirsk, 630090, Russia.

Email: Sihai.Yang@manchester.ac.uk; M.Schroder@manchester.ac.uk

Modulation and precise control of porosity of metal-organic frameworks (MOFs) are of critical importance to their materials function. Here we report the first modulation of porosity for a series of isoreticular octacarboxylate MOFs, denoted MFM-180 to MFM-185, *via* a strategy of selective elongation of metal-organic cages. Owing to the high ligand connectivity, these MOFs show absence of network interpenetration, robust structures and permanent porosity. Interestingly, activated MFM-185a shows a record high BET surface area of 4734 $m^2 g^{-1}$ for an octacarboxylate MOF. These MOFs show remarkable CH_4 and CO_2 adsorption properties, notably with simultaneously high gravimetric and volumetric deliverable CH_4 capacities of 0.24 $g g^{-1}$ and 163 v/v (298 K, 5-65 bar) recorded for MFM-185a due to selective elongation of tubular cages. Dynamics of molecular rotors in deuterated MFM-180a-d_{16} and MFM-181a-d_{16} were investigated by variable-temperature ^2H solid state NMR spectroscopy to reveal the re-orientation mechanisms within these materials. Analysis of the flipping modes of the mobile phenyl groups on the linkers, their rotational rates and transition temperatures, paves the way to controlling and understanding the role of molecular rotors through organic linker design within porous MOF materials.

\body

Metal-organic frameworks (MOFs) are an emerging class of porous, multifunctional materials showing great potential in a wide range of applications.[1–7] Given their metal-organic hybrid nature, MOFs have an exceptionally high degree of structural diversity and tailorability.[8] Thus, not only is the on-demand design of materials that incorporate pores of precise shapes and dimensions achievable, but also the inner surface of these materials becomes a platform for incorporating desirable functionality for target applications.[9,10] Within the field of gas storage, there is a strong correlation between the material porosity and the maximum adsorption capacity. A common strategy to increase porosity in MOFs consists of targeting a framework topology and systematically elongating the linkers to generate additional pore space. This approach has shown success in a number of MOF systems, but is not without drawbacks. For example, increases in porosity typically correlate to increases in pore diameters, which can be detrimental to the strength of host-guest interactions at low surface coverage.[11] Also, often, simple ligand-elongation will ultimately lead to framework interpenetration with reduced porosity and/or stability.[12-14] Powerful driver therefore exists to find the ideal compromise between high porosity and strong host-guest interactions over a wide range of pressures.

The use of rigid, highly-connected linkers (*e.g.* with 6-8 coordinating functions) affords potentially a more robust and stable platform for the development of isoreticular porous materials. This strategy has been widely implemented for $\{Cu\}_2$ paddlewheel systems with hexacarboxylate linkers of C_3-symmetry to generate a family of ***rht***-type MOFs with high and predictable porosity.[15-17] In contrast, effective modulation of porosity for isoreticular MOFs based upon 8-connected linkers has not been achieved to date,[18-26] thus representing a significant synthetic challenge. We report herein the first modulation of porosity in a series of isoreticular octacarboxylate MOFs. By varying the length and nature of the heteropolyaromatic cores of the linkers, we have selectively extended the length of metal-organic cages ongoing from MFM-180 to MFM-185 along one direction, effectively avoiding framework interpenetration. The resulting increase in porosity of the materials does not impair their stability towards activation, and the fixed diameter of the pores allows efficient packing of gas molecules across a wide range of pressures. The dynamics of molecular rotors (*e.g.*, phenyl rings) within MOF materials is a key property to their functionalisation as they form part of the internal pore surface and are thus highly sensitive to the presence of guest molecules.[27-31] In this regard, the series of MOFs herein offer a unique platform to probe the influence of altering the ligand structure on the molecular dynamics and rotational freedom within the resultant framework. To the best of our knowledge, only a few attempts have been made to elucidate the rotational dynamics of linkers in porous MOFs[32-34] and none control them *via* linker design only. We report here the temperature-dependent ^2H NMR studies of selectively deuterated MFM-180-d_{16} and MFM-181-d_{16} to define the rotational and flipping modes of the phenyl groups within these structures in the solid state and the molecular factors that govern these dynamics.

RESULTS AND DISCUSSION

Design and synthesis of octa-connected ligands and isoreticular MOFs. The series of octa-connected linkers, ranging from 19 to 30 Å in dimension, are shown in Figure 1 and their syntheses are described in details in SI. H_8L^0, H_8L^3 and H_8L^5 were synthesized by direct Suzuki-Miyaura coupling of diethylisophthalate-5-boronic acid with the corresponding tetrahalides: 1,1,2,2-tetrakis(4-bromophenyl)ethane, 2,3,7,8-tetrakis(4-bromophenyl)pyrazino[2,3-g]quinoxaline, and 2,3,9,10-tetrakis(4-bromophenyl)-[1,4]dioxino[2,3-g:5,6-g']diquinoxaline for H_8L^0, H_8L^3, and H_8L^5, respectively. In the case of H_8L^1 and H_8L^2, we employed a different strategy where the extended 3',5'-bis(ethoxycarbonyl)biphenyl-4-ylboronic acid was coupled with 1,2,4,5-tetrabromobenzene and 2,3,6,7-tetraiodonaphthalene, respectively. Attempts to prepare H_8L^4 from naphthalene-2,3,6,7-tetraamine failed, and therefore the target MOF MFM-184 was analysed *in silico* based upon the isoreticular nature of this series of materials in this study. Solvothermal reactions of H_8L^0, H_8L^1, H_8L^2 or H_8L^3 with $CuCl_2$ in a mixture of DEF/ethanol/0.1M aqueous HCl (2/2/1, v/v/v) at 80 °C for 16 h afforded the solvated materials $[Cu_4(L^n)(H_2O)_4]_\infty \cdot$ solv or MFM-18n (n = 0, 1, 2, 3). Due to the insolubility of H_8L^5 in the above solvent mixture, the synthesis of MFM-185 was conducted in a mixture of DMF/DMSO/2M aqueous HCl (40/20/1, v/v/v) with $Cu(NO_3)_2 \cdot 2.5H_2O$ for 4 days. The "indirect" synthesis of $[Cu_4(L^0)(H_2O)_4]_\infty$ has been reported *via* transmetallation of the iso-structural $[Zn_4(L^1)(H_2O)_4]_\infty$ complex, in which Zn(II) ions are gradually replaced by Cu(II) ions.[35]

Analysis of the crystal structures. The X-ray single crystal structures of MFM-180, -181, -182, -183 and -185 confirm the formation of square planar $[Cu_2(O_2CR)_4]$ nodes bridged by the octacarboxyate linkers to afford 3D open structures. MFM-180 crystallizes in the tetragonal space group $I\bar{4}2m$ with a = 18.6924(2) Å and c = 35.9196(4) Å. The octacarboxylate linker $[L^0]^{8-}$ is comprised of a central tetraphenylethylene core bearing four isophthalate moieties in 4,4',4'',4''' positions and acts as a 4-connected node (Figure 1). Each isophthalate arm is orthogonal to the main plane of the molecule and acts as a 3-connected node. Each linker connects to eight $[Cu_2(O_2CR)_4]$ paddlewheels, and each paddlewheel connects to four independent linkers. As a result, the MFM-180 framework can be regarded as a 3,3,4-c ***tbo*** net (Figure S1) of stoichiometry (3-c)$_4$(4-c)$_3$ with the corresponding point symbol of $\{6^2.8^2.10^2\}_3\{6^3\}_4$.[36] The metal-ligand linkage affords three types of metal-organic cages (A, B, and C with a ratio of 2:1:1), the smallest of which is an elongated octahedral cage A comprising two ligands and four $[Cu_2(O_2CR)_4]$ paddlewheels (Figure 2). The $[Cu_2(O_2CR)_4]$ moieties occupy the four equatorial vertices while two ethylene groups from the ligands occupy the apical vertices. The overall structure results from the corner-sharing assembly of these octahedral cages A *via* ethylene groups along the c axis and $[Cu_2(O_2CR)_4]$ paddlewheels along the a/b axis. This arrangement generates two types of elongated cuboctahedra cages, each one comprising four ligands and eight $[Cu_2(O_2CR)_4]$ paddlewheels (Figure 2). The largest spheres that can fit within these cages taking into account the van der Waals radii of surface atoms have diameters of 3.0, 13.2 Å and 10.4 Å for cages

A, B and C, respectively. In Cage B, the open metal sites of the paddle-wheels point to the centre of the cavity, whereas in cage C they are tangential to the cavity.

In previously reported examples of octacarboxylate MOFs with **tbo** or **scu** nets,[18-26] the linkers presented a central four-connected node with increasing distances between the central node and four isophthalate moieties. Although this strategy produced isoreticular MOF structures, no increase of porosity was observed, presumably because of flexibility issues and/or highly strained frameworks. As an alternative approach to simply extending the linker length along all directions, we sought to target the extension of specific dimensionalities and lengths to better control the porosity of resultant MOFs. The distance l_1 (Figure 1) is crucial for the formation of the octahedral cages A because it codes for the overall structural assembly. In contrast, the distance l_2 defines the length of cages B and C, and thus we sought to design linkers in which l_1 remains constant but l_2 is augmented. For this purpose, we replaced the four-connected ethylene bond from the ligand H_8L^0 with a series of extended aromatic cores. The targeted isoreticular MOFs (except for MFM-184) were obtained as single crystals and their structures confirmed by single crystal X-ray diffraction.

Replacement of the ethylenyl core in MFM-180 with a benzene ring affords MFM-181 which crystallizes in a different tetragonal space group *I4/mmm*. The change in space group is due to the presence of structural disorder in MFM-181, in which the free rotating phenyl rings are disordered over two positions generated by the mirror symmetry. Nonetheless, MFM-181 exhibits the same **tbo** topology as MFM-180 (Figure S1) when the phenyl core is considered as a four-connected node. The octahedral cage A in MFM-181 is retained as expected. Cages B and C in MFM-181 are elongated along the *c* axis by 2.65 Å in comparison with MFM-180. The size of linkers $[L^2]^{8-}$, $[L^3]^{8-}$ and $[L^5]^{8-}$ is further increased by incorporating central cores with naphthalene, three- and five-fused heteroacenes, respectively. The corresponding MOFs, MFM-182, MFM-183 and MFM-185, all crystallize in the space group *I4/mmm* with the same structure. Given the extension of the polyaromatic cores of $[L^2]^{8-}$, $[L^3]^{8-}$ and $[L^5]^{8-}$, the most accurate topological description of the underlying nets of MFM-182, MFM-183 and MFM-185 reflects a process called "decoration" in which a net vertex is replaced by a group of vertices. Thus, MFM-182, MFM-183 and MFM-185 present the same previously unreported 3,3,4-c net with point symbol: $\{6.10^2\}\{6^2.8^2.10^2\}\{6^3\}_2$ which is derived from the **tbo** net by decoration of half of its 4-c vertices by a pair of 3-c vertices (Figure S1). The calculated accessible voids (PLATON) are 71.5%, 71.2%, 73.3 %, 75.4 % and 76.7 % for MFM-180, MFM-181, MFM-182, MFM-183 and MFM-185, respectively.

Modulation of porosity and gas adsorption property. Prior to activation (involving removal of both the free and coordinating solvents from the pores), the materials were exchanged with methanol. This was followed by heating the solvent-exchanged samples at 100 °C under dynamic vacuum to give activated MFM-180a and MFM-181a. In order to prepare activated MFM-183a and -185a, supercritical CO_2 drying was employed to maximise the retention of their pore structure. MFM-180a, -181a, -183a, and 185a show BET surface areas of 2610, 3100, 4130 and 4730 $m^2 g^{-1}$, respectively, as

determined from N_2 adsorption at 77 K. The BET surface areas for MFM-182a and MFM-184a are predicted by GCMC methods to be 3557 and 4289 m^2 g^{-1}, respectively, because of the difficulty in their bulk synthesis (see SI). Analysis of the N_2 isotherms using a nonlocal density functional theory (NLDFT) model revealed the pore size distribution centered around 13.3, 13.7, 14.3, and 16.3 Å for MFM-180a, -181a, -183a and 185a, respectively. Total pore volumes of 1.00, 1.36, 1.45 and 1.65 cm^3 g^{-1} were obtained from the N_2 isotherms, and compare favourably with that calculated based upon single crystal structure (1.09, 1.19, 1.40 and 1.59 cm^3 g^{-1} for MFM-180a, -181a, -183a and -185a). Additionally, there is a good agreement between experimental and predicted BET surface areas (Figures S4-S15) and overall, the results confirm the complete activation of these MOFs and are consistent with the increasing pore dimensions across the series. To the best of our knowledge, MFM-185a possesses the highest BET surface area and pore volume among octacarboxylate MOFs.

The CH_4 adsorption capacities of MFM-181a, -183a, and 185a are among the highest reported values for the best behaving MOFs at 35 bar, 298 K (Figure 3). Interestingly, the intrinsic trade-off between gravimetric and volumetric capacities is minimised in this series of MOFs owing to the high framework connectivity and thus relatively high crystal density in comparison to other highly porous MOFs. For example, both gravimetric and volumetric CH_4 adsorption capacities of MFM-181a, -183a, and 185a are higher than those reported for the more porous octacarboxylate MOF PCN-80a (17.7 wt %, 142 v/v) under same conditions.[1] CH_4 adsorption in MFM-181a is saturated at 55 bar, whereas MFM-183a and 185a can accommodate more CH_4 molecules at higher pressures owing to their extended pore space. At 65 bar, the total gravimetric uptake of MFM-185a is sufficiently high (29.0 wt %) to compensate for its low crystal density and hence it displays the highest volumetric CH_4 uptake (198 v/v) of the series. Since MFM-181a, 183a and 185a have almost identical CH_4 uptakes at 298 K and 5 bar, the desirable improvement of the materials porosity through elongation of the metal-organic cages affords an increase in both gravimetric and volumetric "working capacities" (defined as the difference in total uptake between 65 and 5 bar). For example, MFM-185 shows the highest deliverable CH_4 capacity in both gravimetric and volumetric terms among all octacarboxylate MOFs (Table S6).

The CO_2 adsorption isotherms were recorded at 298 K up to 20 bar for MFM-180a, -181a, -183a, and 185a (Figure 3). The isosteric heats of CO_2 adsorption were estimated to be around 23 kJ mol^{-1} for all MOFs (Table S7). At low pressure (1 bar), both gravimetric and volumetric CO_2 uptakes are higher for the less porous frameworks, ranging from 13.0 wt % (32.2 v/v) for MFM-185a to 15.0 wt % (54.9 v/v) for MFM-180a, which suggests that a high density of open metal sites is crucial to maximise the low pressure CO_2/framework interactions. For pressures higher than 10 bar, the larger pore volume of MFM-185a allows it to reach the highest gravimetric uptake (107.3 wt % at 20 bar) of the series whereas MFM-181a shows the highest volumetric CO_2 uptake (292.4 v/v at 20 bar) due to its combination of large surface area and moderately low density. These uptakes compare favourably

with other octacarboxylate MOFs presenting higher (PCN-80a[25] : 72.8 wt % at 20bar, 293 K) or similar (MFM-140[18] : 91.2 wt % at 20 bar, 298 K) porosities.

^{2}H NMR studies on dynamics of molecular rotors. Solid-state ^{2}H NMR technique was applied to investigate the molecular dynamics of the rotational aromatic rings in this series of MOFs. MFM-180a and MFM-181a were partially deuterated by selectively introducing D-atoms on the rotational aromatic rings in the ligands to give MFM-180a-d$_{16}$ and MFM-181a-d$_{16}$ (see SI). Variable temperature ^{2}H NMR spectroscopic studies for MFM-180a-d$_{16}$ and MFM-181a-d$_{16}$ (Figure 4 and SI for full spectral data) show that the mobility of the phenyl groups for both materials evolves with temperature starting from a Pake-powder pattern with quadrupolar coupling parameters ($Q_0 = 176$ kHz, $\eta = 0$) typical for static phenyls C-D groups at low temperature (100 K). The evolution of the line shape with rising temperature depicts a re-orientation mechanism similar for both MOFs with three regimes. (i) From low temperatures (100 K) up to T$_1$, the line shape evolves to a typical two-site exchange pattern.[37] (ii) Above T$_1$, the line shape remains stable up to T$_2$, and (iii) above T$_2$ it evolves to yield a narrowed uniaxial Pake-pattern ($Q_1 = 21$ kHz ~ $Q_0/8$, $\eta = 0$), indicating that the phenyl fragments rotate homogeneously around the C_2 axis. Although the uniaxial ligand rotation in MOFs has been reported[35], the complex dynamic behavior in MFM-180a-d$_{16}$ and MFM-181a-d$_{16}$ has not been observed previously.

The striking difference between MFM-180a-d$_{16}$ and MFM-181a-d$_{16}$ lies in the temperatures of transition from one motional mode to another, from two-site flipping to continuous rotation. For MFM-180a-d$_{16}$, T$_1$ is ~ 310 K and T$_2$ is ~ 330 K, while in MFM-181a-d$_{16}$, T$_1$ is ~ 200 K, and T$_2$ remains at 330 K. This result indicates that changes in the ligand core affect only one of the two rotational modes, with the flipping mode that evolves below T$_1$ being notably faster for MFM-181a-d$_{16}$. Significantly, this is the first time such observation has been made in MOFs and opens up the possibility to design the rotational potential of mobile fragments within such porous materials.

The line shape interpretation is based on the following general considerations. The position of mobile phenyl groups in the framework leaves freedom only for rotation or flipping about the C$_2$ axis and the angle between the rotation axis and the C-D bond is naturally fixed to be $\theta_{ph} = 60°$ (Figure 5a). Therefore, the simplest model that can describe the line shape evolution is the four-site jump-exchange rotation for the torsional angle φ covering the whole 360° range (Figure 5b). In such a scheme each of the two C-D bonds flips between two sites ($\varphi_1 <> \varphi_2$ and $\varphi_3 <> \varphi_4$) displaced by a jump angle $\Delta\varphi_1$. When the temperature conditions are met and the phenyl ring is able to overcome the second rotational barrier between the sites $\varphi_1 <> \varphi_3$ and $\varphi_2 <> \varphi_4$ each C-D bonds begins to perform the full 360° rotation. In each pair only the highest barrier is relevant, and thus the motion can be described by the two independent rate constants k_1 and k_2. This model is evidenced by its excellent fit of the experimental data for both samples (Figure 4). The two-site exchange motion governing the line shape below T$_2$ allows the determination of the exact position for C-D bond sites. For MFM-180a-d$_{16}$, the jump angle $\Delta\varphi_1^{\mathrm{I}} = 71°$, while for MFM-181a-d$_{16}$, $\Delta\varphi_1^{\mathrm{II}} = 68°$. The second jump angle can then be

readily computed as $\Delta\varphi_2^i = 180^\circ - \Delta\varphi_1^i$. This shows that the equilibrium positions are displaced compared to an ideal C_4 symmetry. The line shape evolution above T_2 fully supports the four sites exchange model and excludes any other interpretation of the observed spectra. Most intriguing are the potential barriers and collision factors involved. In all cases, the rotation rates follow the standard Arrhenius law (Figure 6). For k_1 in MFM-180a-d$_{16}$ the parameters are $E_1 = 26$ kJ mol^{-1} and $k_{10} = 1.6 \times 10^{11}$, and for MFM-181a-d$_{16}$ $E_1 = 20$ kJ mol^{-1} and $k_{10} = 9 \times 10^{11}$. For k_2 in MFM-180a-d$_{16}$ $E_2 = 28$ kJ mol^{-1} and $k_{20} = 3 \times 10^7$, while for MFM-181-d$_{16}$ $E_2 = 34$ kJ mol^{-1} and $k_{20} = 4.6 \times 10^8$. Additional analysis suggests that intramolecular steric interactions in MFM-180a-d$_{16}$ are stronger. In both cases these interactions are maximized when all phenyls lie in one plane, with three interaction sites and H-D or D-D distances governing the strength of interaction (Figure 5c and 5d). For MFM-180a-d$_{16}$ Site I shows the interaction of two mobile phenyl groups in 1,1' positions of the ethylene core, while for MFM-181a-d$_{16}$ it is the interaction of the mobile fragment with the hydrogen of the aromatic core fragment. Sites II and III are geometrically similar for both materials and the shortest distance is realized for site II (marked blue on Figures 5c and 5d) The rates of the slowest motion k_2 (Figure 6) are almost superimposable for both frameworks and we can thus attribute k_2 to the torsional barrier that rises from electrostatic interaction between neighboring hydrogens in site II. Hence the rate constant k_1 must be governed by site I because the shortest possible distance at the site III is $d_3 \sim 1.9$ Å and is identical in the two linkers, while for site I for MFM-180a-d$_{16}$ $d_1 \sim 1.6$ Å and for the MFM-181a-d$_{16}$ $d_1 \sim 1.9$ Å. The comparison of the first motion rates k_1 for the two materials confirms that they are indeed considerably different: k_1 is much greater in MFM-181-d$_{16}$ than in MFM-180-d$_{16}$. Interestingly while the flipping mode k_1 in both cases is characterized by a collision factor typical for flipping motion in MOFs $\sim 10^{11}$ Hz,[34] for k_2 it is $\sim$ 3 orders of magnitude smaller at $\sim 10^8$ Hz, which reflects the strong influence of the steric restrictions on the axial rotation of the phenyl groups in these linkers. This ^{2}H NMR study has revealed that the complex dynamic behavior of the molecular rotors in MOFs in solid state can be elucidated and thus controlled by establishing a strong correlation between the ligand design and the rotational dynamics, the latter of which is a key property of MOF functionalities.

CONCLUSION

The first series of isoreticular MOF materials based on a family of octacarboxylate linkers has been developed. The rigid, heteropolyaromatic linkers were designed to self-assemble with [Cu$_2$(O$_2$CR)$_4$] paddlewheels to afford frameworks with elongated nano-tubular cages of fixed diameter. The isoreticular design results in systematically increased pore volumes and surface areas for the MOFs. Notably, in the case of CH$_4$ adsorption, extension of the linker causes no uptake loss in the low pressure region, and both gravimetric and volumetric uptakes are simultaneously enhanced at high pressure. This affords an impressive CH$_4$ "working capacity" of 0.24 g g^{-1} and 163 v/v (298 K, 5-65 bar) for activated MFM-185a. We attribute this behaviour to the efficient packing of gas molecules in the tubular pores and the high connectivity (and thus suitably high crystal density) of the framework.

In addition, for the first time, a rational synthetic design has allowed control of the torsional dynamics of linkers in MOF solids. The high predictability of the linker/metal self-assembly combined with their pore shape make this series of MOFs a unique platform for exploring further the tuning of porosity, decoration of pores, and development and control of new molecular rotors in functional MOFs.

References

(1)   He, Y.; Zhou, W.; Qian, G.; Chen, B. *Chem. Soc. Rev*. **2014**, *43*, 5657.

(2)   Zhang, Z.; Yao, Z.-Z.; Xiang, S.; Chen, B. *Energy Environ. Sci.* **2014**, *7*, 2868.

(3)   Yang, S.; Sun, J.; Ramirez-Cuesta, A.J.; Callear, S. K.; David, W. I. F.; Anderson, D.; Newby, R.; Blake, A. J.; Parker, J. E.; Tang, C. C.; Schröder, M. *Nat. Chem.* **2012**, *4*, 887.

(4)   Horcajada, P.; Gref, R.; Baati, T.; Allan, P. K.; Maurin, G.; Couvreur, P.; Férey, G.; Morris, R. E.; Serre, C. *Chem. Rev.* **2012**, *112*, 1232.

(5)   Lee, J.; Farha, O. K.; Roberts, J.; Scheidt, K. A.; Nguyen, S. T.; Hupp, J. T. *Chem. Soc. Rev.* **2009**, *38*, 1450.

(6)   Li, J.-R.; Sculley, J.; Zhou, H.-C. *Chem. Rev.* **2012**, *112*, 869.

(7)   (a) Mondloch, J. E.; Katz, M. J.; Isley III, W. C.; Ghosh, P.; Liao, P.; Bury, W.; Wagner, G. W.; Hall, M. G.; DeCoste, J. B.; Peterson, G. W.; Snurr, R. Q.; Cramer, C. J.; Hupp, J. T.; Farha, O. K. *Nat. Mater.* **2015**, *14*, 512.

(8)   Li, M.; Li, D.; O'Keeffe, M.; Yaghi, O. M. *Chem. Rev.* **2014**, *114*, 1343.

(9)   Alsmail, N. H.; Suyetin, M.; Yan, Y.; Cabot, R.; Krap, C. P.; Lü, J.; Easun, T. L.; Bichoutskaia, E.; Lewis, W.; Blake, A. J.; Schröder, M. *Chem. - Eur. J.* **2014**, *20*, 7317.

(10)   Yang, S.; Ramirez-Cuesta, A-J.; Newby, R.; Garcia-Sakai, V.; Manuel, P.; Callear, S. K.; Campbell, S. I.; Tang, C. C.; Schröder, M. *Nat. Chem.* **2015**, *7*, 121-129.

(11)   Lin, X.; Champness, N. R.; Schröder, M. *Top. Curr. Chem.* **2010**, *293*, 35.

(12)   Batten, S. R.; Robson, R. *Angew. Chem. Int. Ed.* **1998**, *37*, 1460.

(13)   Haldar, R.; Sikdar, N.; Maji, T. K. *Mater. Today* **2015**, *18*, 97.

(14)   Lin, X.; Telepeni, I.; Blake, A. J.; Dailly, A.; Brown, C. M.; Simmons, J. M.; Zoppi, M.; Walker, G. S.; Thomas, K. M.; Mays, T. J.; Hubberstey, P.; Champness, N. R.; Schröder, M. *J. Am. Chem. Soc.* **2009**, *131*, 2159.

(15) Yan, Y.; Lin, X.; Yang, S.; Blake, A. J.; Dailly, A.; Champness, N. R.; Hubberstey, P.; Schröder, M. *Chem. Commun.* **2009**, 1025.

(16)   Nouar, F.; Eubank, J. F.; Bousquet, T.; Wojtas, L.; Zaworotko, M. J.; Eddaoudi, M. *J. Am. Chem. Soc.* **2008**, *130*, 1833.

(17)   Farha, O. K.; Eryazici, I.; Jeong, N. C.; Hauser, B. G.; Wilmer, C. E.; Sarjeant, A. A.; Snurr, R. Q.; Nguyen, S. T.; Yazaydın, A. Ö.; Hupp, J. T. *J. Am. Chem. Soc.* **2012**, *134*, 15016.

(18) Tan, C.; Yang, S.; Champness, N. R.; Lin, X.; Blake, A. J.; Lewis, W.; Schröder, M. *Chem. Commun.* **2011**, *47*, 4487.

(19) Ma, L.; Mihalcik, D. J.; Lin, W. *J. Am. Chem. Soc.* **2009**, *131*, 4610.

(20) Mihalcik, D. J.; Zhang, T.; Ma, L.; Lin, W. *Inorg. Chem.* **2012**, *51*, 2503.

(21) Eubank, J. F.; Mouttaki, H.; Cairns, A. J.; Belmabkhout, Y.; Wojtas, L.; Luebke, R.; Alkordi, M.; Eddaoudi, M. *J. Am. Chem. Soc.* **2011**, *133*, 14204.

(22) Xue, Y.-S.; Jin, F.-Y.; Zhou, L.; Liu, M.-P.; Xu, Y.; Du, H.-B.; Fang, M.; You, X.-Z. *Cryst. Growth Des.* **2012**, *12*, 6158.

(23) Zhuang, W.; Yuan, D.; Liu, D.; Zhong, C.; Li, J.-R.; Zhou, H.-C. *Chem. Mater.* **2012**, *24*, 18.

(24) Wei, Z.; Lu, W.; Jiang, H.-L.; Zhou, H.-C. *Inorg. Chem.* **2013**, *52*, 1164.

(25) Lu, W.; Yuan, D.; Makal, T. A.; Li, J.-R.; Zhou, H.-C. *Angew. Chem. Int. Ed.* **2012**, *51*, 1580.

(26) Spanopoulos, I.; Tsangarakis, C.; Klontzas, E.; Tylianakis, E.; Froudakis, G.; Adil, K.; Belmabkhout, Y.; Eddaoudi, M.; Trikalitis, P. N. *J. Am. Chem. Soc.* **2016**, *138*, 1568.

(27) Kolokolov, D. I.; Jobic, H.; Stepanov, A. G.; Guillerm, V.; Devic, T.; Serre, C.; Férey, G. *Angew. Chem. Int. Ed.* **2010**, *49*, 4791.

(28) Gould, S. L.; Tranchemontagne, D.; Yaghi, O. M.; Garcia-Garibay, M. A. *J. Am. Chem. Soc.* **2008**, *130*, 3246.

(29) Kolokolov, D. I.; Stepanov, A. G.; Jobic, H. *J. Phys. Chem. C* **2014**, *118*, 15978.

(30) Horike, S.; Matsuda, R.; Tanaka, D.; Matsubara, S.; Mizuno, M.; Endo, K.; Kitagawa, S. *Angew. Chem. Int. Ed.* **2006**, *45*, 7226.

(31) Comotti, A.; Bracco, S.; Ben, T.; Qiu, S.; Sozzani, P. *Angew. Chem. Int. Ed.* **2014**, *53*, 1043.

(32) Horike, S.; Matsuda, R.; Tanaka, D.; Matsubara, S.; Mizuno, M.; Endo, K.; Kitagawa, S. *Angew. Chem. Int. Ed.* **2006**, *45*, 7226.

(33) Inukai, M.; Fukushima, T.; Hijikata, Y.; Ogiwara, N.; Horike, S.; Kitagawa, S. *J. Am. Chem. Soc.* **2015**, *137*, 12183.

(34) Comotti, A.; Bracco, S.; Sozzani, P. *Acc. Chem. Res.* **2016**, *49*, 1701.

(35) Wei, Z.; Lu, W.; Jiang, H.-L.; Zhou, H.-C. *Inorg. Chem.* **2013**, *52*, 1164.

(36) Delgado-Friedrichs, O.; O'Keeffe, M.; Yaghi, O. M. *Acta Crystallogr. Sect. A* **2006**, *62*, 350.

(37) Macho, V.; Brombacher, L.; Spiess, H. W. *Appl. Magn. Reson.* **2001**, *20*, 405.

Methods Summary

The ligands H_8L^0, H_8L^1, H_8L^2, H_8L^3 and H_8L^5 were all synthesized using a Suzuki-Miyaura coupling reaction between the corresponding tetrahalogenated core and boronic acid, followed by hydrolysis of the ester functions. The synthesis of H_8L^1 is described in detail in SI. The selectively deuterated linkers were synthesised following the same procedures but starting from deuterated building blocks.

Synthesis of MFM-180, 181, 182, and 183: H_8L^{0-3} (0.30 mmol) and $CuCl_2$ (0.19 g, 1.40 mmol) were dissolved in N,N'-diethylformamide (30 mL). EtOH (30 mL) and an aqueous solution of HCl (0.1M, 15 mL) were added to the resulting solution, which was placed in a tightly capped 250 mL Duran$^®$

pressure plus laboratory bottle (cat. n° 1092234). The solution was heated at 80 °C in an oven for 16 h, and a large amount of crystalline product precipitated. The crystal plates of the correspondind MOF were isolated by filtration while the mother liquor was still warm.

Due to the poor solubility of H_8L^5, MFM-185 was synthesized following slightly different conditions, see SI.

Detailed synthesis procedures and characterizations of the linkers and MOFs, along with crystallographic data and description of gas sorption and solid state ^2H NMR experiments can be found in supporting information.

Supporting Information

Supplementary information is available in the online version of the paper. CCDC 1472806-1472810 contain the supplementary crystallographic data for materials MFM-180, -181, -182, -183 and -185, respectively. These data can be obtained free of charge from the Cambridge Crystallographic Data Centre via www.ccdc.cam.ac.uk/data_request/cif.

Corresponding Author

Sihai.Yang@manchester.ac.uk; M.Schroder@manchester.ac.uk

Author Contributions

Acknowledgments

Competing financial interests

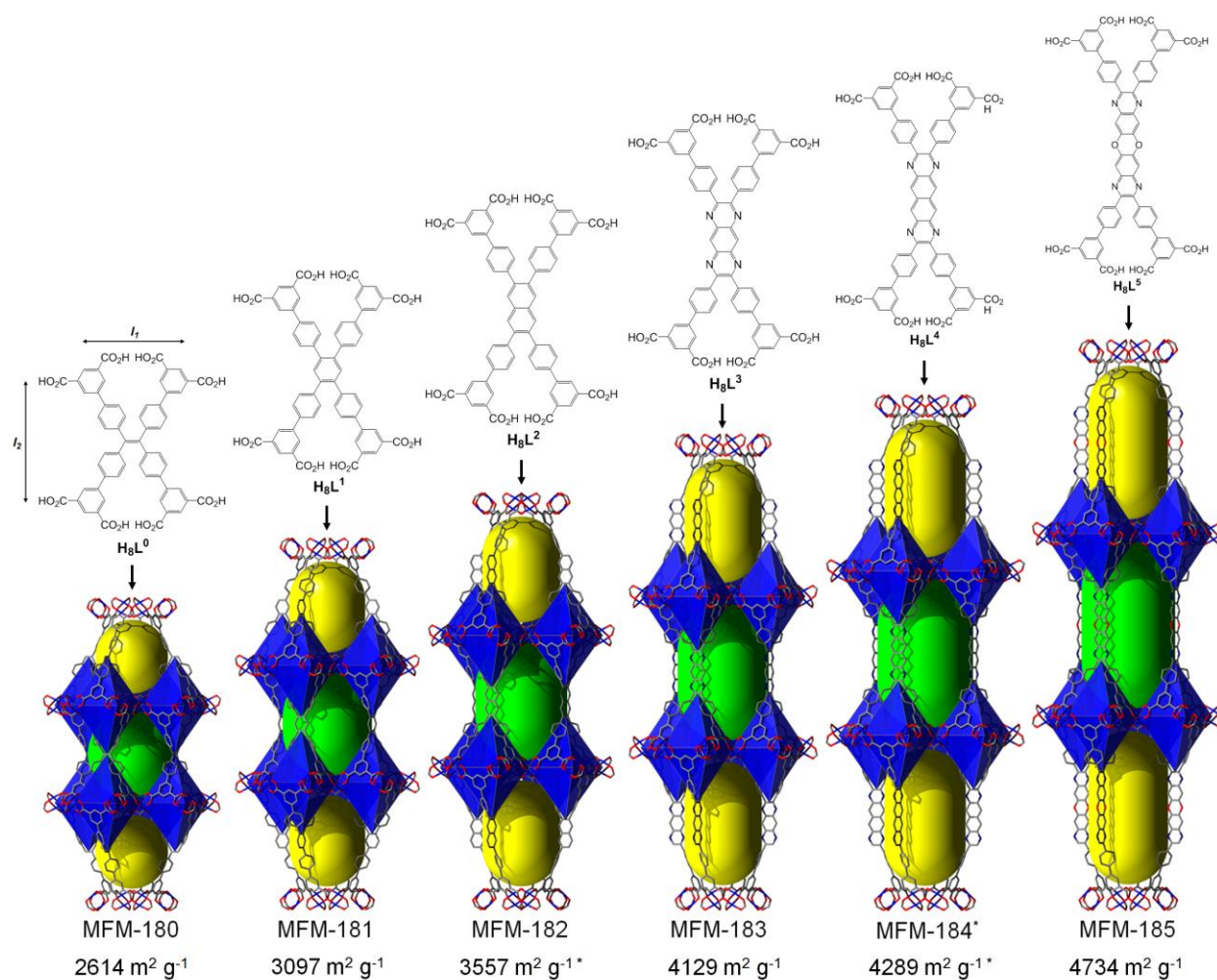The authors declare no competing financial interests.

Schemes and Figures

Figure 1. Chemical structures for the octacarboxylate linkers H_8L^0 to H_8L^5 used for the synthesis of MFM-180 to MFM-185, representation of the cage assembly in MFM-180, MFM-181, MFM-182, MFM-183, MFM-184 (*predicted structure) and MFM-185, and corresponding BET surface areas (*computed).
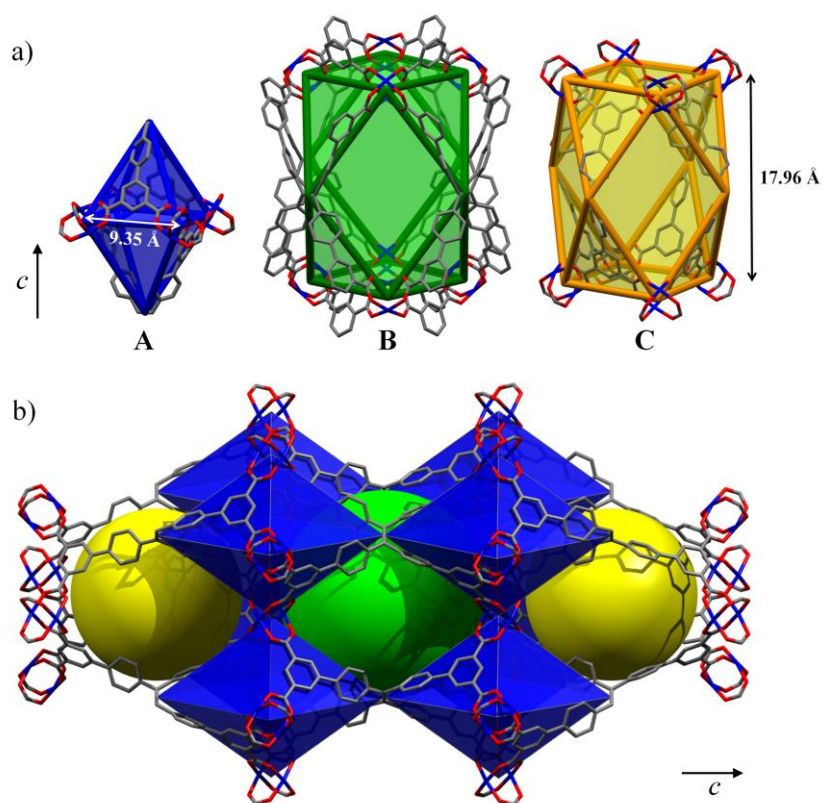
Figure 2. View of a) polyhedral representations of the three types of cages A (octahedral), B and C (cuboctahedral) and b) their three-dimensional assembly in MFM-180.
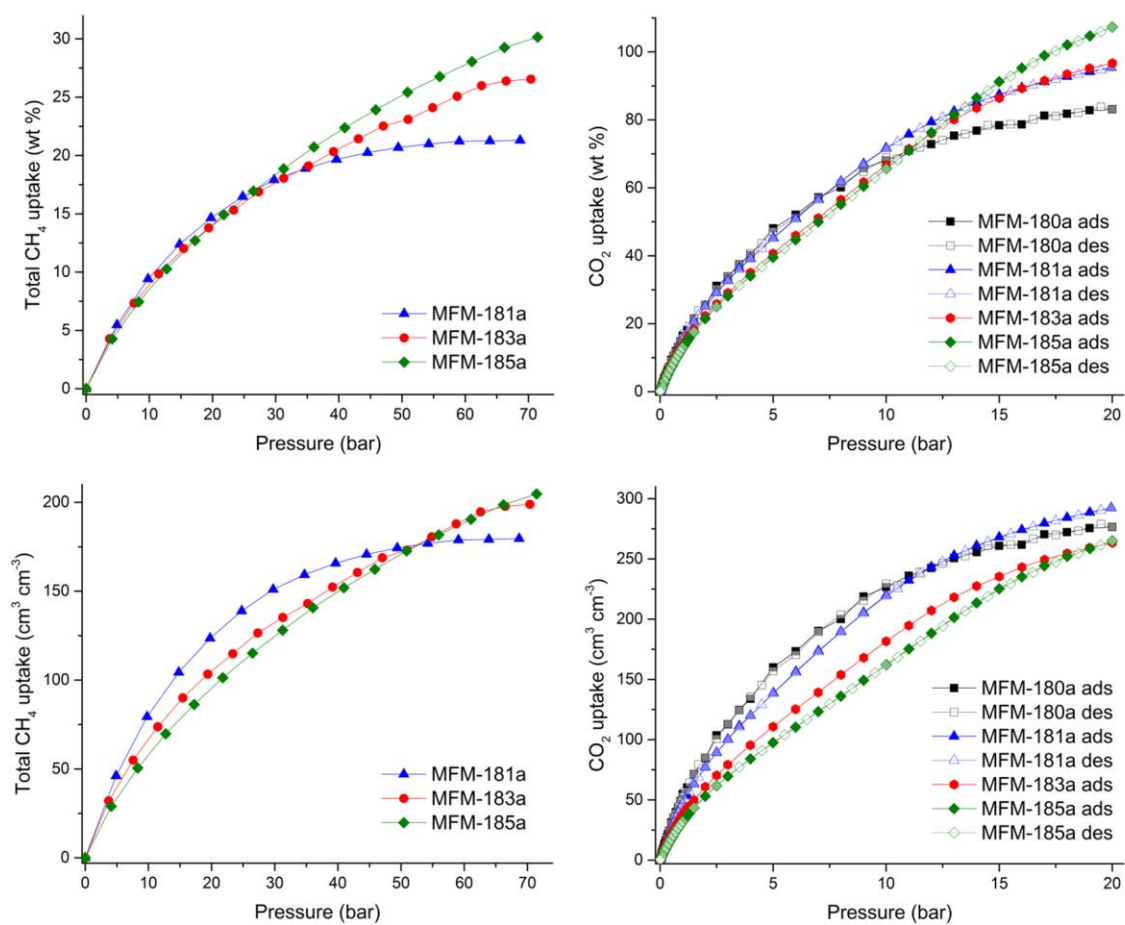
Figure 3. High pressure CH_4 sorption isotherms for MFM-181a, -183a and -185a at 298 K and CO_2 sorption isotherms for MFM-180a, -181a, -183a and -185a up to 20 bar at 298 K. Top: gravimetric uptake; bottom: volumetric uptake.
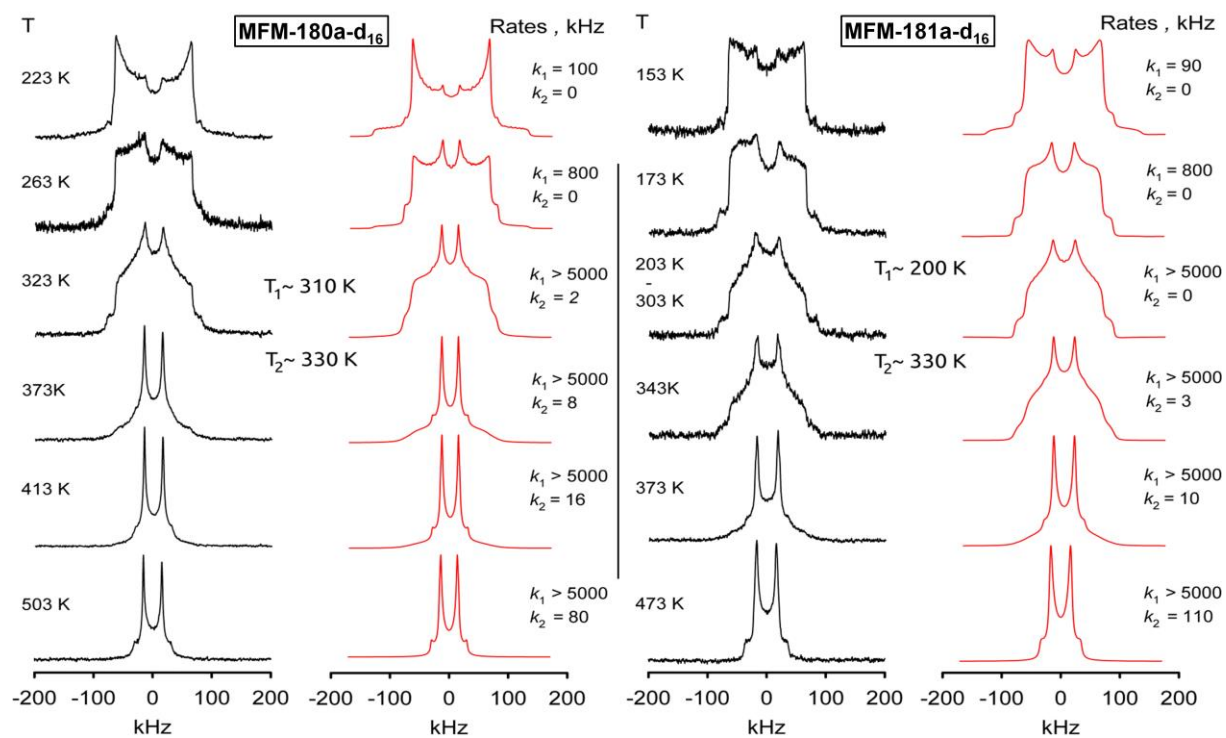
Figure 4. Comparison of the ^{2}H NMR line shape temperature dependence for phenyl fragments in MFM-180a-d$_{16}$ and MFM-181a-d$_{16}$ (experimental – black, simulation - red).
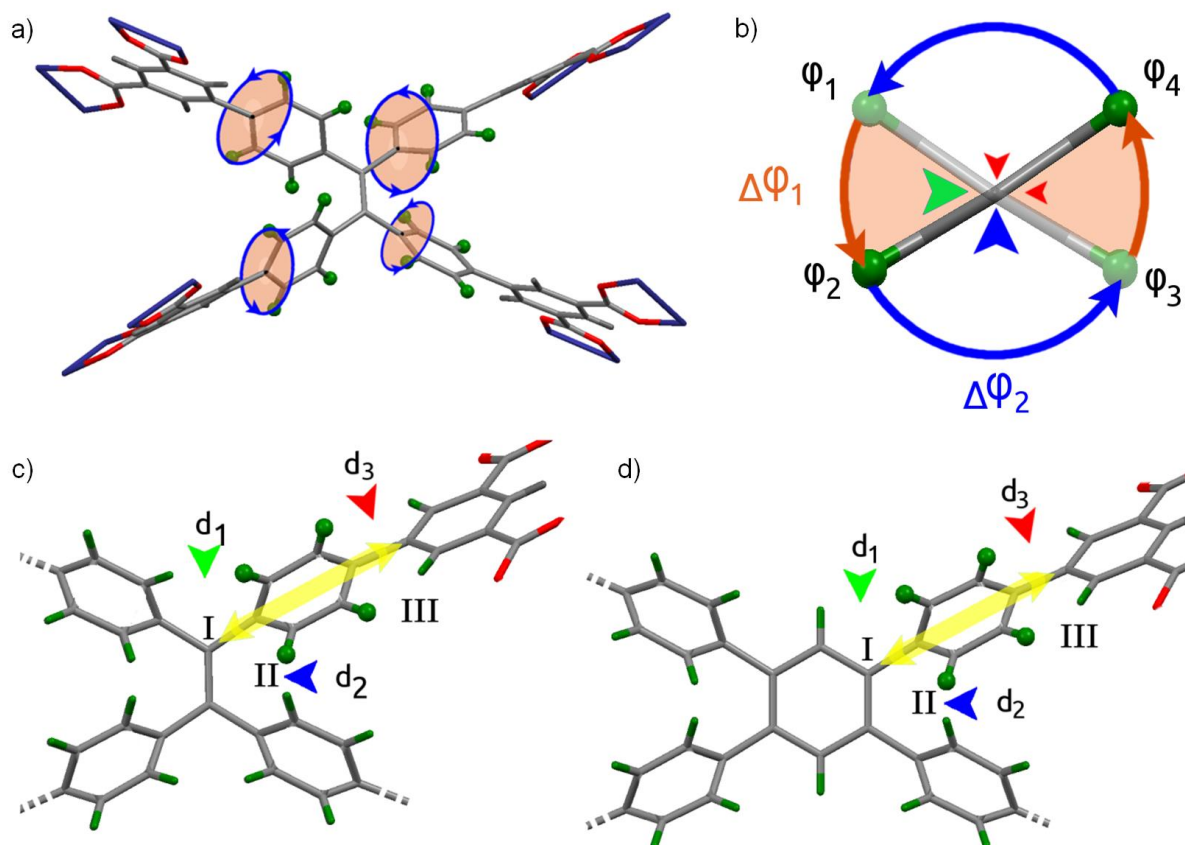
Figure 5. a) Representation of the linker in MFM-180a-d_{16} with its four mobile phenyl rings; b) Scheme of rotation sites for phenyl groups in MFM-180a-d_{16} and MFM-181a-d_{16}. The reorientation scheme comprises a four site exchange motion with two different rate constants: k_1 ($\Delta\varphi_1$) and k_2 ($\Delta\varphi_2$). The green arrow represents the barrier associated with k_1, the blue arrow represents the barrier associated with k_2, and the red arrows are associated with barriers in the $\Delta\varphi_1$ and $\Delta\varphi_2$ regions associated with minor steric restrictions. c) and d) Scheme of interaction sites that might influence the rotational potential for phenyl groups in MFM-180a-d_{16} and MFM-181a-d_{16}, respectively. Parameter d_2 is the shortest achievable distance for the electrostatic interaction between the phenyl hydrogens and is similar in both materials.
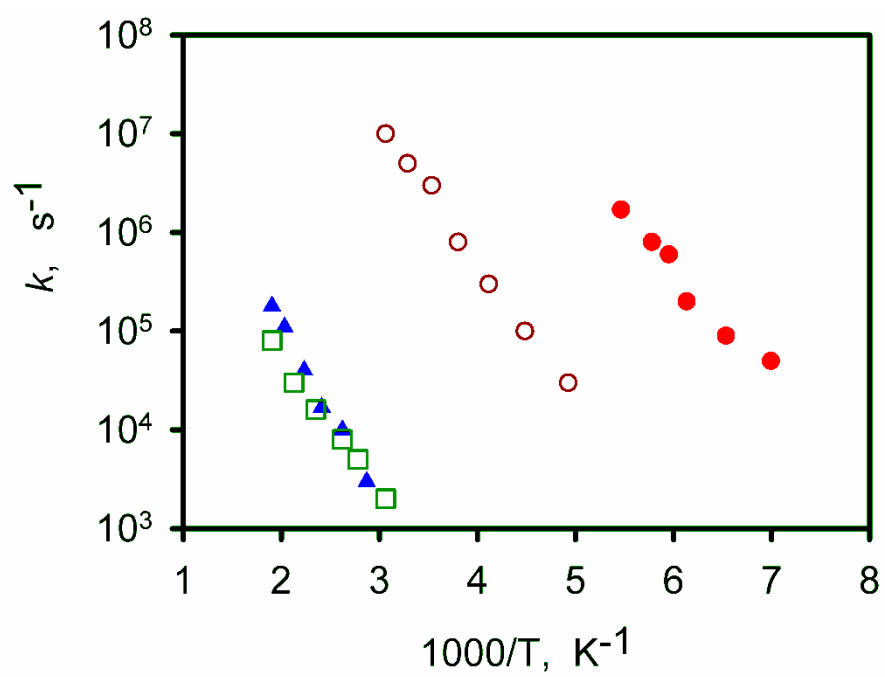
Figure 6. Arrhenius plots of the rotational rate constants k : (○) k_1 and (□) k_2 for MFM-180a-d$_{16}$; (●) k_1 and (▲) k_2 for MFM-181a-d$_{16}$.